BUTTERWORTH HEINEMANN

Flow visualization and heat transfer experiments in a turbulent channel flow obstructed with an inserted square rod

M. Yao and M. Nakatani
Department of Mechanical Engineering Nara National College of Technology, Nara, Japan

K. Suzuki
Department of Mechanical Engineering, Kyoto University, Kyoto, Japan

Flow visualization and heat transfer measurements were made for a turbulent channel flow obstructed with an inserted square rod. The space between the square rod and the duct wall was changed in five steps. Intermittent dye injection method was introduced to visualize the Karman vortex shed from the rod and to track its motion. Hydrogen bubble method was combined to visualize the near-wall flow. The results reveal that the Karman vortex shows criss-cross motion, even when the rod is placed off the center plane. The vortex moves at a speed equal to the cross-sectional averaged velocity. As in a low Reynolds number flow, the washing action of discrete vortices appearing near the wall is suggested as an important key mechanism to produce the enhancement of heat transfer.

Keywords: heat transfer enhancement; intermittent dye injection method; channel turbulent flow; obstruction by a square rod; Karman vortex; Strouhal number; criss-cross motion

Introduction

Enhancement of internal flow heat transfer is of practical importance, and some basic studies have been made for channel flows with an insertion of turbulent promoters (Webb and Bergles 1982; Oyakawa and Mabuchi 1981, 1982; Yao et al. 1988; Liou and Hwang 1992a, 1992b; Hong and Hsieh 1993). However, how the heat transfer enhancement is produced has not yet been clarified. For example, Yao et al. (1988) did a study on a turbulent channel flow disturbed by a staggered array of cylinders and found that, under the condition where pumping power was kept constant, enhancement of heat transfer was most effectively achieved when cylinders were mounted at a position a little detached from the channel wall. In an attempt to simulate this finding numerically a two-dimensional (2-D) numerical computation was made employing a k-ε type turbulence model for a similar but somewhat simpler type of disturbed turbulent channel flow; i.e., a turbulent flow in a channel wherein a single square rod was placed (Yao et al. 1990). The obtained results did not agree well with the experimental data, but the disagreement suggested that periodically changing unsteady flow structure existing behind the rod plays an important role. However, which specific role of the unsteady flow structure produces the heat transfer enhancement has not been studied. The present study aims at experimentally exploring what type of unsteady flow appears downstream of the inserted body and at studying how it is related to the heat transfer enhancement. For simplicity, a square rod is again adopted as a body to disturb a turbulent channel flow.

Apart from the line of study above, one of the present authors did a numerical study for a channel flow obstructed with a square rod in low Reynolds number range over which flow remains steady laminar if the rod is removed (Suzuki et al. 1991a, 1991b, 1991c). In this Reynolds number range, the high vorticity near-wall layer was found to interact with the Karman vortices shed from the rod, intermittently separating and developing into the periodical formation of discrete vorticity islands. These vorticity islands exert "the washing action" to the channel wall and, thus, enhance the wall heat transfer (Suzuki and Suzuki 1994a, 1994b). One of the specific objectives of the present study is to see if a similar picture is applicable to the present higher Reynolds number case. In the low Reynolds number range, Karman vortex was found to show criss-cross motion (Suzuki et al. 1993). Another objective of this study is to see if similar criss-cross motion can occur even in the present higher Reynolds number range where background turbulence exists. To attain these goals, the intermittent dye injection method first proposed by Senoo and Yamaguchi (1975) is applied with an attempt to track the motion of each Karman vortex. Heat transfer measurements are also made in the present study, and the data to be obtained are analyzed in terms of the results of flow visualization.

Experimental apparatus and procedure

Flow visualization was made in an open water channel basically the same as that previously used by Yao et al. (1988). Definitions of several geometric parameters and coordinate systems used are

Address reprint requests to Dr. M. Yao, Department of Mechanical Engineering, Nara National College of Technology, Nara 639-11, Japan.

Received 24 January 1995; accepted 2 June 1995

Int. J. Heat and Fluid Flow 16: 389-397, 1995

655 Avenue of the Americas, New York, NY 10010

0142-727X/95/$10.00
SSDI 0142-727X(95)00047-T

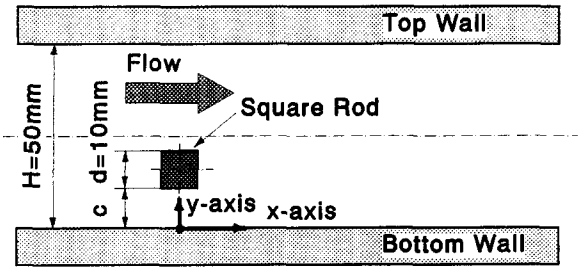

Figure 1 Definitions of geometric parameters and coordinate systems

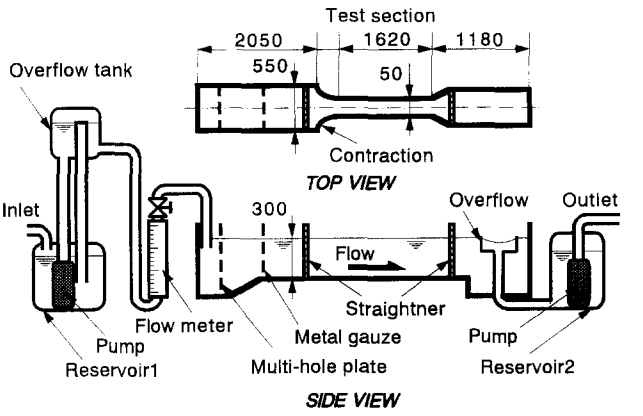

Figure 2 Schematic view of experimental apparatus for flow visualization

described in Figure 1. Figure 2 is a schematic view of the experimental apparatus used in the present flow visualization. More detail of the test section is presented in Figure 3. A square rod was vertically inserted into an open water channel at a stream-wise position of 1,000 mm downstream from the inlet to the test section. The cross-stream position of the rod was changed variously, and, in the following discussion, it is expressed with a clearance ratio defined as $y' = 2c/(H-d)$. Here, d is the rod thickness, H the width of the channel, and c the space between the square rod and the channel wall. D was kept equal to 10 mm, and H was equal to 50 mm in all the present experiments. Main flow visualization was made within the stream-wise region from $x = -5$ mm to $x = 250$ mm ($x/H = 5$) in a horizontal layer of 10-mm vertical thickness; i.e., from 240 mm to 250 mm high from the bottom of the channel or from 50 mm to 60 mm deep from the free surface. The depth of water flow was kept constant in all runs at about 300 mm in the test section.

The velocity profiles of approaching flow to the rod obtained in a horizontal plane and in a vertical plane, respectively, are shown in Figure 4. In this experiment a hydrogen bubble method was used, and the Reynolds number was Re = 10,500. Approaching flow was confirmed to be basically uniform along the vertical direction; therefore, 2-D, as is shown in Figure 4b. Figure 4a suggests that the approaching flow was not in a fully developed state at the insertion position of the square rod. However, whether the approaching flow was fully developed or not did not produce a serious change in the flow characteristics downstream of the rod. This was because the flow field was completely disturbed by the rod itself, as shown later. The disturbed flow field was still basically 2-D. This is also described later.

Two methods were used for flow visualization, namely hydrogen the bubble method and the dye injection method. The hydrogen bubble technique was primarily applied to study the basic feature of the unsteady flow near the channel wall. For this purpose, it was combined with the intermittent dye injection method (described later), and hydrogen bubble lines were then repeatedly produced at an interval from a thin platinum wire mounted in a horizontal plane. The streamwise position of the bubble-generating wire was changed variously to widen the visualized region.

Two types of dye injection method were used in the present study; i.e., a normal one and an intermittent dye injection method. The normal type of dye injection method was used to check the flow two-dimensionality. Two injection needles were aligned in a vertical plane near the rod, directing their outlet ports downstream. The top views of the two streak lines looked statistically similar. They did not significantly deflect in the vertical direction. Thus, it was suggested that two dimensionality of the disturbed flow was basically preserved upstream of the position $x/H = 4$. Noticeable flow three-dimensionality was suggested to evolve downstream of the position of $x/H = 4$. The Karman vortex starts to break up into smaller 3-D eddies in that region.

The intermittent dye injection method was developed to investigate the motion of the Karman vortex and the flow structure downstream of the square rod. The key point of this method is that the dye is introduced into the flow at a timing appropriate for a certain duration in order to visualize a specific flow structure only. The system used in the intermittent dye injection method is illustrated in Figure 3. A watered solution of condensed milk was adopted as the dye and was periodically introduced into the flow field through an injection hole drilled on the front surface of the square rod near its leading edge. The timing, time interval, and

Notation

Cp	coefficients of static pressure drop $2\Delta p/\rho U_m^2$
c	clearance between square rod and duct wall, mm
d	size of square rod, mm
f	shedding frequency of the Karman vortex, 1 s
H	height of the duct, mm
h	local heat transfer coefficient, W/m^2K
Nu	local Nusselt number, $2hH/\lambda$
q	wall heat flux, W/m^2
Re	Reynolds number, $2U_mH/\nu$
Re^*	Reynolds number, U_m^*d/ν
St^*	Strouhal number, fd/U_m^*
U_m	mean streamwise velocity, m/s
U_m^*	cross-sectional average velocity in the space between the rod and the channel wall, m/s, $U_mH/(H-d)$
V_h	moving speed of Karman vortex, m/s
x	streamwise distance measured downstream from the center of the square rod, mm
y	distance measured from the lower channel wall, mm
y'	clearance ratio, $2c/(H-d)$
z	spanwise distance, mm

Greek

Δp	static pressure drop, Pa
λ	thermal conductivity of the fluid, W/mK
ν	kinematic viscosity of the fluid, m^2/s
ρ	density, kg/m^3

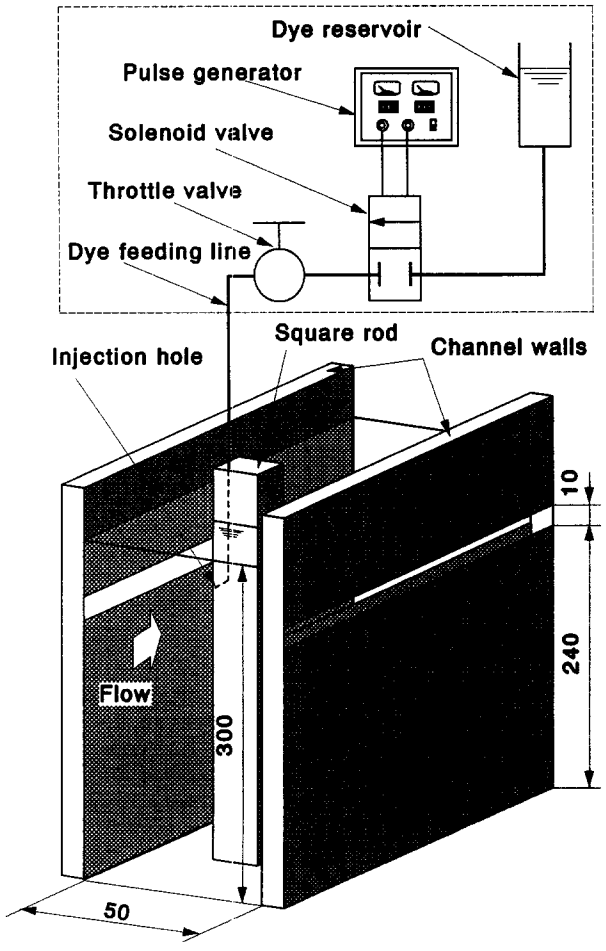

Figure 3 Detail of test section and apparatus for intermittent dye injection method

time duration of dye injection were controlled by a magnetic solenoid valve connected to the dye-feeding tube. An electric pulse signal of small width generated by a pulse generator was used as a signal to control the valve. The time interval between consecutive pulses was adjusted so that the dye was injected synchronous with the Karman vortex shed from the rod. Two square rods were provided; one having the injection hole at a position close to the upper edge (rod A), and another having the hole close to the lower edge (rod B). Here, lower side means the side closer to the channel wall under discussion and upper side means the other side. In the following, the vortex shed from the upper half of the rod is called "vortex A" and another from the lower half "vortex B."

The small width electric pulse signal was used to maintain a short injection time. A short injection time duration was preferred for several reasons. With a short injection time duration, either vortex A or vortex B could be dyed, depending on whether rod A or rod B was being used. Karman vortex consists of two parts; i.e., its core region and its outer region, and the two regions differ in nature from each other. The core region directly obtains fluid mass from the separation bubble behind the rod and is characterized by solid rotation. On the other hand, the outer region grows in size by entraining fluid mass from the main flow and behaves somewhat like the irrotational flow around a vortex (Hans 1983). With the present intermittent dye injection method, dye was introduced directly into the layer adjoining the rod surface that develops into the core region of the vortex. Therefore, the core region was easily dyed with a short time duration of dye injection. Dye could penetrate into the outer region but only by the diffusion effect. Diffusion of dye is likely to proceed slowly and nonuniformly. Therefore, dyeing all parts in the outer region was difficult. Even if it were possible, dye would have to have been injected in an excessive amount, thus, over a long time duration. Then, not only the outside region of one vortex, but also its neighboring vortex would have been dyed together. Thus, the diffusion effect would make the visualized image of the vortex blurred at its rim. On the other hand, determination of the center position of the vortex would be possible when only the core region was dyed. Therefore, a short injection time duration was preferred in tracking the motion of the vortex.

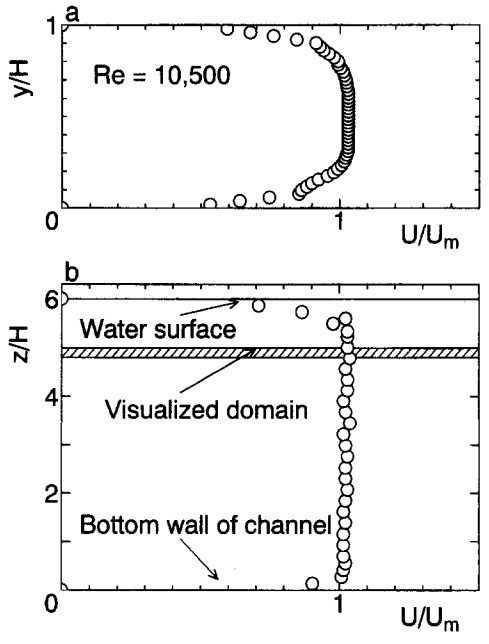

Figure 4a Velocity profile without an insertion of rod (horizontal plane); *b* velocity profile without an insertion of rod (vertical plane)

In additional experiments, especially when the hydrogen bubble method was combined, all the vortices shed both from the upper and lower sides of the square rod were dyed by applying electric pulses having larger width or with longer injection time duration. With excessively longer injection time duration, even the region outside a vortex was dyed.

A picture of the unsteady flow field was recorded with a video camera and replayed later for detailed analysis. Both a wide view and a close-up view were recorded. The wide-view record was used to examine whether the criss-cross motion of the Karman vortex appears or not and to see how the vortex behaves in the downstream region. The close-up view was used in discussion of near-wall flow structure. It was also used for the quantitative analysis of the motion of the Karman vortex; i.e., for the

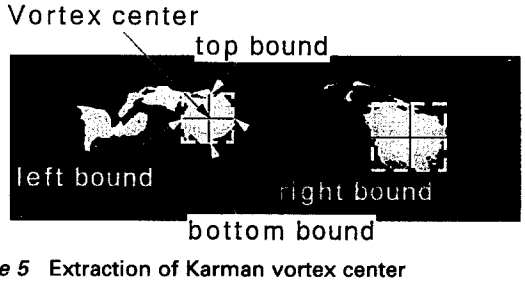

Figure 5 Extraction of Karman vortex center

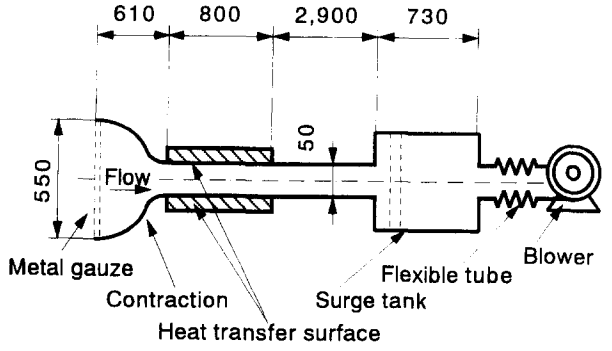

Figure 6 Schematic view of experimental apparatus for heat transfer

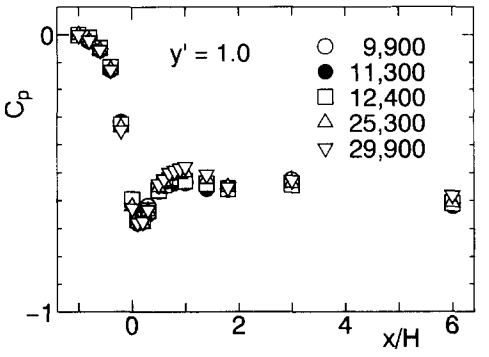

Figure 7 Stream-wise distribution of *Cp* (effect of Reynolds number)

measurement of its moving speed and shedding frequency. In the close-up view, one pixel of the video monitor corresponds to the visualized actual area of 0.6×0.6 mm of the flow field. As is shown in Figure 5, the close-up image of each vortex was first intensified and then the measured positions of the left, right, top, and bottom side boundaries of each vortex were digitized. The center position of each vortex was determined as the center of a rectangle whose every side lines fit the digitized side boundaries of the vortex. Uncertainty U_{RSS} of the flow visualization was calculated from errors in the positioning of the vortex center relative to the wall position, in measurements of flow rate, and in the uncertainty related to the minimum resolution of video the monitor. Results of the uncertainty analysis revealed that $U_{RSS}/H = 6.7\%$ in the close-up view case, and $U_{RSS}/H = 9.1\%$ in the wide-view case.

To supplement the results of the flow visualization, static pressure was also measured along the channel wall. For this purpose, another test section with 19 static pressure taps of 0.5-mm inner diameter were provided along its center line. The measured data of static pressure are presented in the form of pressure loss coefficient or in the nondimensional form of the difference Δp between the first pressure tap and each of the other taps.

Figure 6 is a schematic view of the experimental apparatus used in heat transfer experiments (Yao et al. 1988). Heat transfer experiments were conducted using an open-circuit wind tunnel having a 400-mm width and a 50-mm height. In previous studies, heat transfer measurement was made for fully developed turbulent flow conditions (Yao et al. 1988, 1994). In those cases, the test section was preceded by a 4000-mm-long entrance section. This entrance section was removed in the present experiment to establish a velocity profile at the inlet similar to that in the flow visualization experiments. However, this change did not have an essential effect on heat transfer characteristics, as discussed later. Eight stainless steel sheets with 50-mm width and 25-μm thickness were glued carefully onto both of the inner surfaces of the duct walls. The gap between the neighboring sheets was kept as small as possible. All sheets were connected electrically in series and heated by passing an alternating electric current through them. For the measurement of wall temperature, more than 70 alumel-chromel thermocouples of 0.1-mm thickness were attached to the back surface of the sheet glued close to the centerline of the channel walls. The thermal leakage due to the heat conduction toward the back side of the channel wall was at a maximum 15% of electric heating power input. This was evaluated by making use of one-dimensional (1-D) heat-conduction equation and was taken into account in correction of the wall heat flux. For this purpose, the temperature of the outside surface of the channel wall was also measured at nine stream-wise positions with thermocouples. The amounts of heat loss were almost uniform along the flow direction, and the radiative heat transfer from the duct wall surface was estimated at about 1% of the total heat supply.

Results and discussion

Distribution of static pressure

Streamwise distribution of the static pressure measured for the case of $y' = 1.0$ is shown in the form of pressure loss coefficient *Cp* in Figure 7. The distribution of *Cp* remains almost similar in shape, regardless of the flow Reynolds number. This suggests that the time-averaged flow field near the channel wall does not significantly vary with a change of Reynolds number. Therefore, the following discussion of the flow structure at the Reynolds number of about 10,000 may be applicable to other cases of different Reynolds number. One characteristic of the results is the existence of a noticeable adverse pressure gradient behind the rod. This large adverse pressure gradient suggests the occurrence of flow separation there. The stream-wise position of separation point does not significantly vary with the change of Reynolds number. Stream-wise distributions of the static pressure loss coefficient *Cp* are presented in Figure 8 for the five cases of $y' = 0.0$, 0.2, 0.4, 0.7, and 1.0. The Reynolds number in this experiment was Re = 11,300. In contrast to the small effect of Re on the distribution of *Cp*, the effect of y' is significant. It indicates that the flow pattern varies noticeably with the change of the space between the rod and the channel wall.

Motion of Karman vortex

Figure 9a shows the time series of the video images of vortex A visualized with the intermittent dye injection method for the case where Re = 10,500, and $y' = 1.0$. In this case, the vortex was

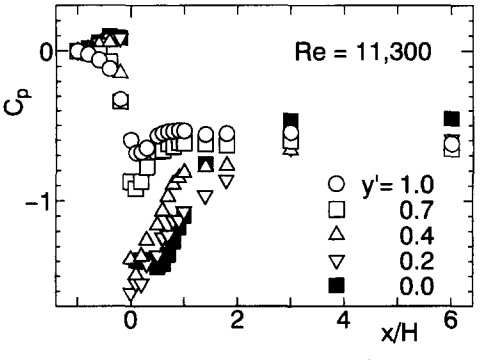

Figure 8 Stream-wise distribution of *Cp* (effect of y', Re = 28,600)

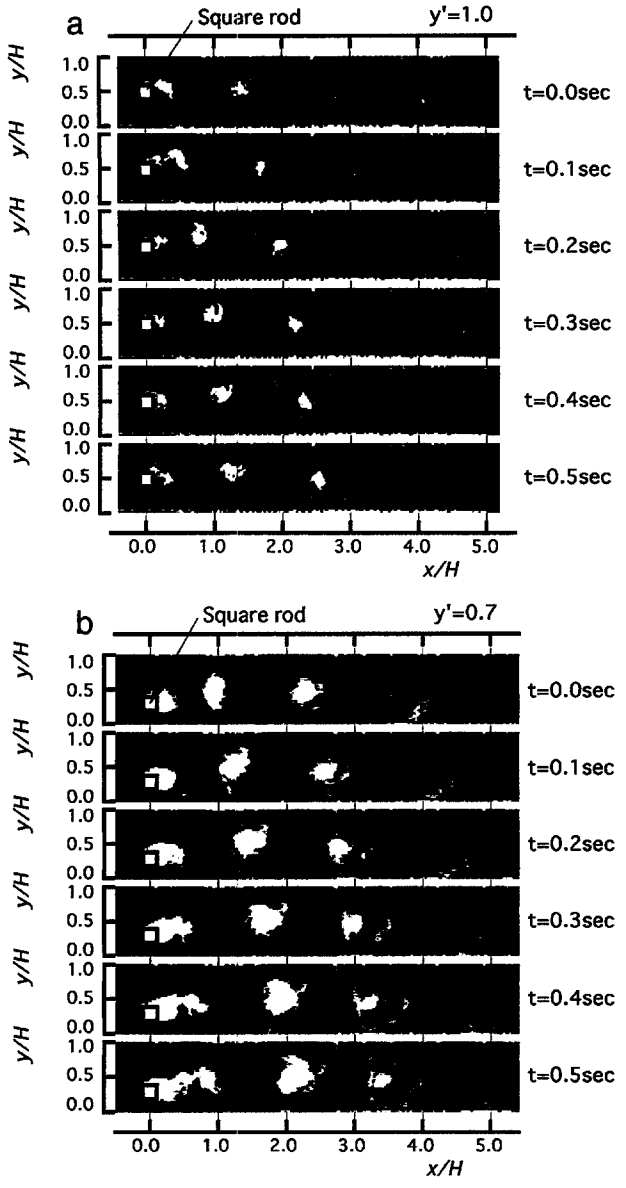

Figure 9a Flow visualization by intermittent dye injection method ($y' = 1.0$, Re = 10,500); *b* Flow visualization by intermittent dye injection method ($y' = 0.7$, Re = 10,500)

regularly shed from the rod and each photograph was taken at an interval of almost one-sixth of the time period of vortex shedding. The rod was placed in the center plane of the channel. Therefore, the time-averaged flow field should be symmetric with respect to the center plane of the channel. In contrast, the presented instantaneous photographs of vortex A only do not certainly show any symmetry.

Figure 9b shows the time series of the images of vortex A visualized at the same Reynolds number Re = 10,500 but in the case of $y' = 0.7$. In this case, the vortex was still regularly shed from the rod, and the recorded images were taken at almost every one-sixth of the time period of vortex shedding. Since the rod was placed off the center plane in this case, the time-averaged flow field was asymmetric with respect to the center plane. In accordance with this asymmetry, the vortex B was much smaller in size compared to vortex A and moved upward rapidly after its shedding. It should have been shed from the rod between the two instants when the bottom and top frames were recorded. As

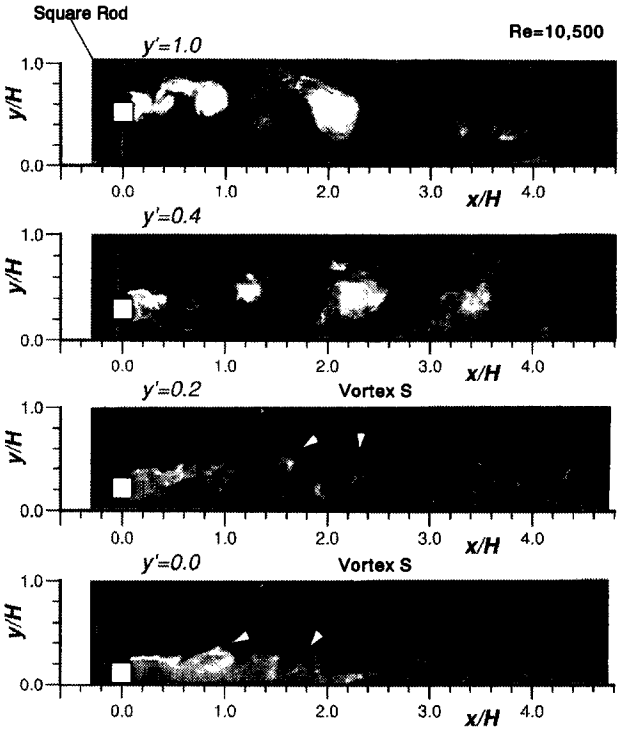

Figure 10 Flow visualization by intermittent dye injection method (effect of y', Re = 10,500)

observed in the figure, dye remains in the separation bubble behind the rod at such instants. However, vortex B cannot be observed at all in the photographs. This suggests that vortex B did not obtain fluid mass from the separation bubble behind the rod but only from the separation shear layer adjoining the lower side of the rod where dye was not introduced in this particular experiments.

At the positions where $x/H < 2.0$, the dyed vortex slowly grows in size, but at positions downstream of $x/H = 2.0$, a more noticeable change of the dyed vortex occurs. The dyed part expands outward more rapidly and the dye fades away rather quickly. Both phenomena proceed owing to the mixing at its

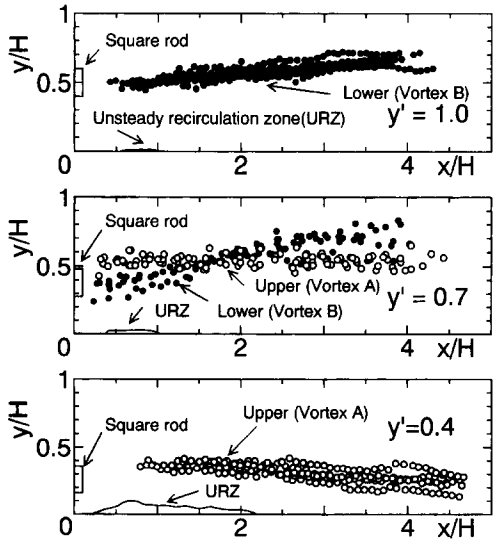

Figure 11 Center position of Karman vortex (Re = 10,500)

brim. Thinning of the dye color proceeds quickly, in particular after x/H 4.0. This is partly due to the three dimensionality of the flow, which becomes more noticeable in this region. Three dimensionality of the flow may generate stronger mixing. After the position of $x/H = 5.0$, the dye completely fades away. The photographs taken with the intermittent dye injection method for four cases of $y' = 0.0$, 0.2, 0.4, and 1.0 are compared with each other in Figure 10. These photographs were obtained again at Re = 10,500. In this case, dye was injected for a little longer duration. Thus, dye spread over much wider region than in Figure 9a, and it is observable even in the near-wall region. This suggests that the Karman vortex can interact with the near-wall region, even in the case where $y' = 1.0$, and enhancement of wall heat transfer can be expected to occur then.

Criss-cross motion of Karman vortex

Periodic shedding of the Karman vortex occurs in the cases where $y' \geqq 0.4$, as is easily confirmed in Figure 10. For such cases, the center position of the vortex was measured in each frame of the video records. The obtained data are plotted in Figure 11. The symbols ○ and ● indicate the results of vortex A and vortex B, respectively. In the case where $y' = 1.0$, the flow field should be symmetric in a statistical sense so that results are plotted only for vortex B. Measurement of the center position was made for 10–20 vortices for each case but only some of those data are presented in the figure to avoid unnecessary duplication of the data. Noticeable spread of the obtained data is partly due to the irregularity characteristic to the intense background turbulence, due to the inaccuracy related to the incomplete spread of dye within the core region of vortex, and due to the inaccuracy in sizing of the vortex. Despite the spread of the data, an important conclusion can be drawn from the plotted data.

At a low Reynolds number, periodically changing, well-organized unsteady flow is generated downstream from a rod (Suzuki et al. 1991a, 1993a). The Karman vortex shed from the rod was found then to show the criss-cross motion; the vortex shed from the upper half of the rod crossed the center plane and moved toward the bottom wall of channel, and another from the lower half of the rod approached the top wall of channel. In Figure 11, Vortex B is clearly observed to cross the center plane of the channel when $y' = 1.0$. Therefore, criss-cross motion of the Karman vortex is actually confirmed to occur, even when flow is in a turbulent flow regime. In the case where $y' = 0.7$, paths of vortices A and B are clearly found to intersect each other around the streamwise position $x/H = 1.7$. Therefore, asymmetry of the flow geometry does not suppress the criss-cross motion of the Karman vortex as was observed at low Reynolds number (Suzuki et al. 1993b).

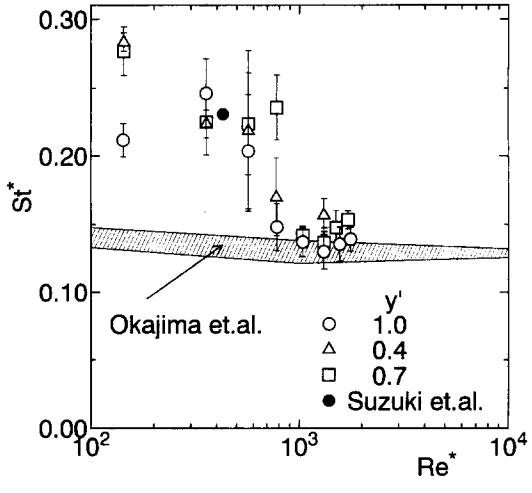

Figure 12 Strouhal number

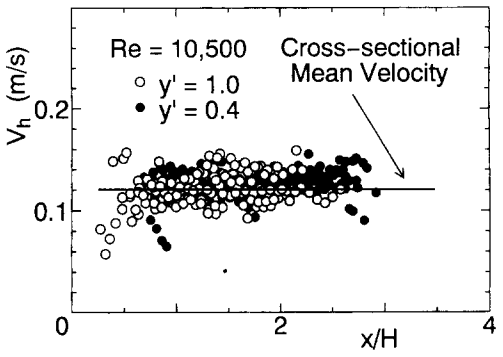

Figure 13 Moving speed of Karman vortex

In the case where $y' = 0.4$, only the results for vortex A are plotted. In this case, as already pointed out for the case of $y' = 0.7$, vortex B is much smaller in size, moves upward more rapidly, and is easily affected by the motion of vortex A, which is much larger in size. Therefore, it is very difficult to track the motion of vortex B accurately. This is why the positions of vortex B are not plotted in the figure. However, the plotted path of vortex A indicates that it crosses the horizontal line passing through the center of the rod. Therefore, the generation of the criss-cross motion is also suggested in this case. $y' = 0.4$ is the smallest clearance ratio at which periodic unsteady flow is observed. In cases where $y' = 0.0$ and 0.2, it is observed that the separation shear layer formed on the upper side of the rod becomes unstable, and it rolls up into a series of discrete vortices. The vortices thus formed approach the channel wall. However, the formation of a discrete vortex is not very periodic. These photographs are discussed again in connection with the heat transfer data.

Shedding frequency and moving speed of vortex

Shedding frequency of the Karman vortex was determined by measuring the interval between the two instants when successive vortices arrive at a stream-wise location. The obtained results are plotted in Figure 12 in the form of Strouhal number St*. Rod size d and cross-sectional average velocity in the space between the rod and the channel wall U_m^* are used in the definitions of St* and Re*. The present data obtained in low Reynolds number range, where flow remains periodical and well organized, agree fairly well with the numerical result obtained by Suzuki et al. (1993a), while they are clearly higher than the experimental data obtained by Okajima (1982) for the case where a rod was placed

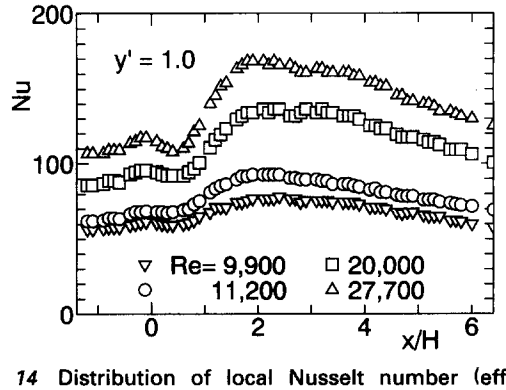

Figure 14 Distribution of local Nusselt number (effect of Reynolds number)

in a uniform unconfined flow. On the other hand, at higher rod Reynolds number range of $Re^* \geq 1{,}000$, the value of St^* is only a little higher than the results by Okajima. Figure 13 shows the moving speed V_h of the Karman vortex obtained in the present study. The speed was determined by measuring the traveling distance of the vortex during the time interval between two successive frames (1/15 s) of video record. In the figure, V_h is observed constant over a wide range of streamwise positions after $x/H = 0.5$ and is equal to the cross-sectional mean velocity. The same was observed for other cases of different Reynolds number and of different value of y'.

Heat transfer characteristics

Heat transfer data are now discussed. First, attention is given to the results obtained with the channel having the short entrance section or with uniform flow at the inlet. Figure 14 shows the streamwise distribution of the measured local Nusselt number for four cases of different Reynolds number Re = 9900, 12,000, 20,000, and 27,700. It is observed in the figure that Nu distribution remains almost similar in shape, regardless of the Reynolds number. This is consistent with the fact that the distribution of *Cp*, the pressure loss coefficient, showed similar shape, regardless of the Reynolds number. Therefore, the discussion of heat transfer enhancement is given below only for the results obtained at Re = 11,200.

Figure 15a shows the distributions of the local Nusselt numbers obtained for five clearance ratios $y' = 0.0$, 0.2, 0.4, 0.7, 1.0, and at the Reynolds number Re = 11,200. Two symbols ○ and ● present the data for the upper and lower channel walls, respectively. Figure 15b shows the data obtained previously at Re = 10,500 (Yao et al. 1994); the distributions of the local Nusselt numbers obtained with the channel having a long entrance section or in a channel where the inlet flow was in turbulent fully developed state. Comparing Figures 15a and 15b, the values of Nu are different between the two cases of different inlet flow conditions. In particular, the third peak is more remarkable in Figure 15b than in Figure 15a. However, the peak positions of Nu are found to be little affected by the difference in the inlet flow condition. Therefore, the following qualitative discussion for the heat transfer mechanism is based on the flow visualization in a channel having short entrance section, but the discussion may be applicable also to the data obtained under the inlet condition of a fully developed turbulent flow. The results presented in Figure 15a are discussed in the following, giving attention only to the results on the lower wall (the data illustrated with symbol ●). Heat transfer enhancement is more noticeably achieved on this wall, because it is located closer to the rod.

In the illustrated Nu distributions, three peaks are observable. Since discussion is concentrated later on the second peak, brief discussion is given now on the first and third peaks. A mild peak appears around $x/H = 0$ in all the cases except for $y' = 0.0$. This first peak of Nu is generated due to the flow acceleration incurred in the space between the square rod and the channel wall. Its peak value becomes largest in the case of $y' = 0.2$; i.e., the case where the space between the rod and the wall is smallest.

In the cases where $y' \leq 0.2$, a noticeable peak also appears in the distribution of Nu. The peak position is more upstream when $y' = 0.0$ than when $y' = 0.2$. However, the peak position of $y' = 0.0$ is located downstream the second Nu peak position of $y' = 0.4$. Referring to Figure 15b, the peak of Nu under the discussion looks equivalent to the third peak of Nu in the distribution for $y' = 0.4$. We now discuss how the third peak is generated. The streamwise position of the third peak moves upstream with a decrease of y'. It corresponds to the position where the separation shear layer starting from the upper front edge of the rod approaches most closely to the lower channel wall. In the separation shear layer, discrete vortices (Vortices S)

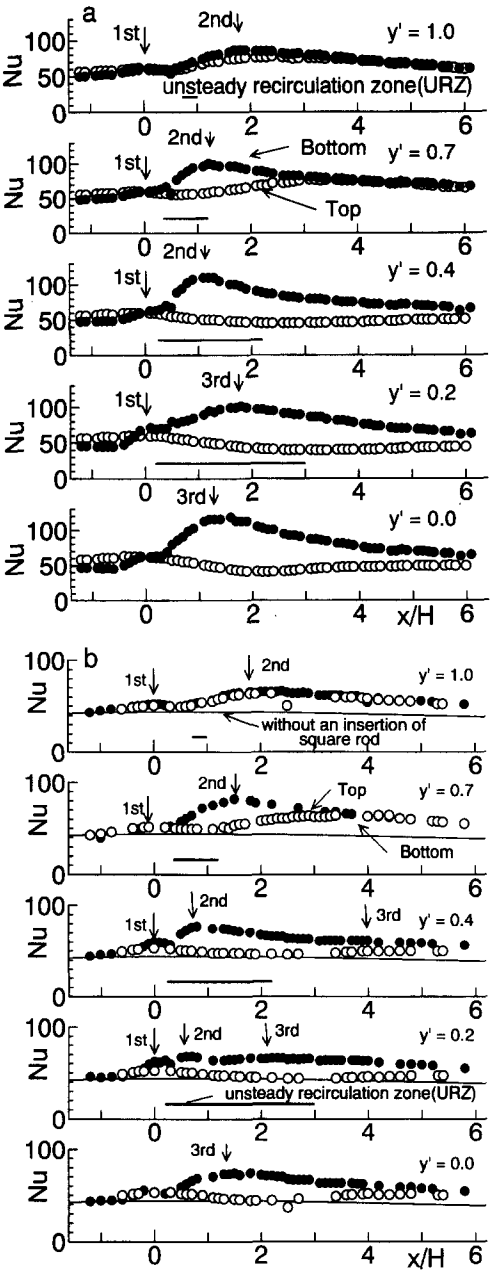

Figure 15a Distribution of local Nusselt number (effect of clearance ratio, Re = 10,500, undeveloped entrance condition); *b* Distribution of local Nusselt number (effect of clearance ratio, Re = 10,500, fully developed entrance condition)

are formed one after another and approach the channel wall, as was shown in Figure 10. These vortices S are the same in nature as vortex A in the sense that they are characterized by negative spanwise vorticity. Thus, each of the vortices S induces clockwise fluid motion around it and entrains fresh or cooler fluid from its downstream side to the space between itself and the channel wall, as is suggested by Suzuki et al. (1991c). This fluid entrainment has the effect of spontaneously making the temperature gradient at the wall large and, therefore, the effect of instantaneously augmenting the wall heat transfer. This is called the washing action by Suzuki and Suzuki (1994a). The third peak is generated by the repeated approach of the vortices S to the near-wall region and by their repeated exertion of the washing action to the wall.

Generating mechanism of the second Nu peak

We now turn our attention to the second peak of Nu distribution. Its appearance is the primary cause of the heat transfer enhancement achieved by the insertion of the rod. It appears at a more upstream position when the clearance ratio y' is reduced, and the value of the second peak becomes largest when $y' = 0.4$. These are in accordance with the findings of Oyakawa and Mabuchi (1981) and Yao et al. (1988) for the turbulent channel flows with an insertion of a staggered array of cylinders. This supports the idea of studying the mechanism of heat transfer enhancement with insertion of a single rod in place of an array of turbulence promoters. Oyakawa and Mabuchi (1981) presented a picture for the heat transfer enhancement. They suggested that the wall heat transfer was enhanced by the intense turbulence produced by the interaction between the side vortex and vortex A shed from the rod. The interaction between the side vortex and vortex A includes their merging into one vortex and the breaking down of the merged vortex into turbulence. From their description, the side vortex they referred to should be equivalent to the vorticity island more clearly identified by Suzuki et al. (1991c) for low Reynolds number flow. A presently observed and important fact is that vortex A continues to exist over a long distance and that its breaking down does not occur upstream of $x/H = 4.0$, as confirmed in Figure 9b for the case of $y' = 0.7$. However, as already discussed, the second peak of Nu appears at $x/H = 1.8$ in that case, the position well upstream of $x/H = 4.0$. Vortex A and the vorticity island have the same sign of vorticity. Thus, if the discrete vorticity island merges into vortex A, the merged vortex should not break down easily. On the contrary, vorticity should then be reinforced in the merged vortex (Hans 1983). For these reasons, the picture presented by Oyakawa and Mabuchi (1981) is difficult to accept.

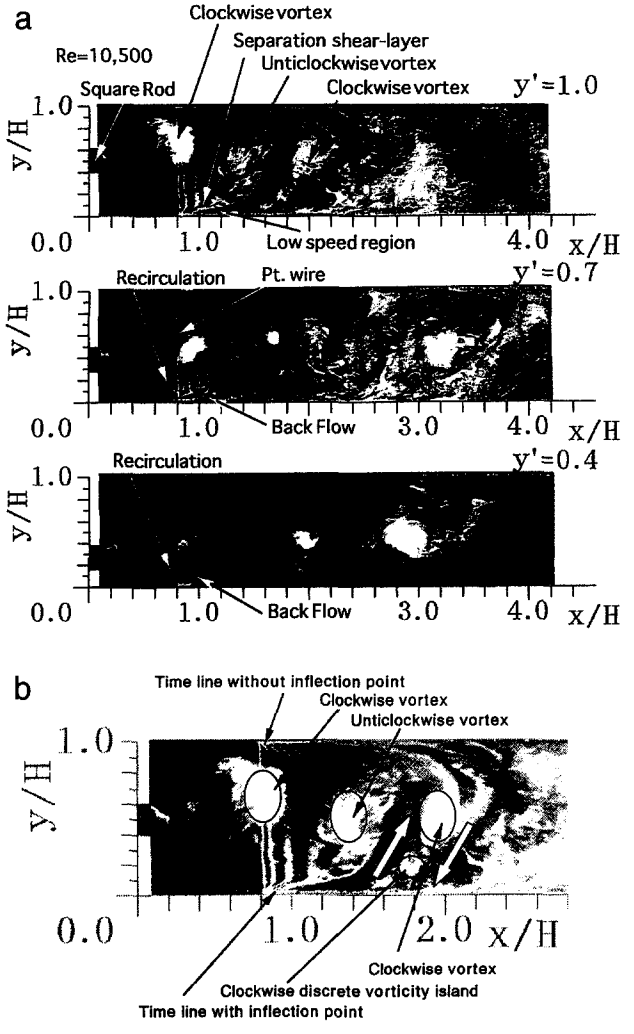

Figure 16a Flow visualization by the intermittent dye injection method and hydrogen bubble method (Re = 10,500); *b* Partial magnification of photograph in case of $y' = 1.0$

Vortex A approaches toward the bottom channel wall due to the criss-cross motion and may directly cause the enhancement of heat transfer. However, this direct effect of vortex A is rather weak when the clearance ratio y' is not as small. As already discussed for cases where $y' = 0.0$ and 0.2, the direct effect of vortex A should be the cause of the third peak of the Nu distribution and is not the cause of the second Nu peak. The most probable heat transfer mechanism for the second Nu peak is, again, that given by Suzuki and Suzuki (1994a, 1994b) for similar flow at much lower Reynolds number; namely, the washing action exerted by the discrete vorticity island.

The reason for this conjecture is now discussed based on some results of the present flow visualization. Figure 16a shows the photographs taken for the three cases of different value of y' and Figure 16b is the partial magnification of the photograph taken in the case of $y' = 1.0$. These figures show the results of the flow visualization made by using the intermittent dye injection method together with the hydrogen bubble method simultaneously. In these experiments, dye was injected over a longer time duration than that used in the normal intermittent dye injection method. As a result, dye remains in the rear region of the rod even after the shedding of vortex A has been completed. Thus, vortex B was also dyed in these photographs. In the case where $y' = 1.0$ (Figure 16b or top photograph in Figure 16a), the inflection point of the bubble lines is observed to exist near the lower channel wall. This indicates that a low velocity region exists near the wall. On the other hand, there is no inflection point in the bubble lines formed near the upper channel wall. If the flow is statistically symmetric and changes periodically, flow structure observed in the upper side of the channel is the one to be realized after a half cycle of flow fluctuation in the lower side of the channel. This is the case of the present flow in principle. Thus, it can be easily imagined that appearance and disappearance of low velocity region occur alternatingly near the wall in one cycle of the flow fluctuation. Flow in the low-speed region is normally directed downstream but is sometimes directed upstream. The appearance of back flow is confirmed by the bubble lines deflected upstream from the platinum wire located at $x/H = 0.8$, as is found in Figure 16a. This fluctuation of flow direction occurs due to the irregularity characteristics to turbulent flows. In the cases where $y' = 0.4$ and 0.7, appearance of back flow was regularly observed. The bubble lines with the inflection point indicates that the spanwise vorticity instantaneously becomes largest at a position off the channel wall, while the normal bubble lines without inflection point observed at another instant indicates that the vorticity becomes largest at the wall. Thus, the vorticity at one point near the wall is indicated to be periodically fluctuating in magnitude. This strongly suggests that the near-wall flow structure under the present discussion is similar to the counterpart at much lower Reynolds number studied by Suzuki et al. (1994a, 1994b). In their case, a high-vorticity wall layer intermittently separates from the wall downstream of the rod, and its downstream tip protrudes toward the center plane of the channel. The protruded tip is disconnected after a while and develops into a vorticity island (Suzuki et al. 1991c). Each vorticity island induces a clockwise circular fluid motion around it and a backflow appears in the region between the vorticity island and the wall. Although there is no direct support for the formation of such a vorticity island in the present case, the periodical fluctuation of the vorticity at a position off the channel

wall and the appearance of the low velocity region near the wall fit the picture described by Suzuki et al. (1994a, 1994b). The backflow region near the wall can be regarded as the result of the clockwise fluid motion induced by a vorticity island above it. Thus, its appearance can be a footprint of the formation of a vorticity island above it. The region where backflow is intermittently observed is indicated in Figure 15 as "URZ" (unsteady recirculating zone). In this particular survey, the wire location was changed variously along the stream-wise direction. The position of URZ indicated in Figure 15 does not completely coincide with the position of the second peak of Nu distribution, as observed in Figure 15, but they roughly agree with each other. Backflow does not necessarily appear over the whole indicated region simultaneously. The backflow region itself moves downstream after its onset toward its downstream end at its disappearance. Therefore, rough agreement between the two positions is enough to accept the heat transfer mechanism suggested by Suzuki et al. (1994a) as the most probable one for the present flow.

Concluding remarks

Flow visualization was made for a turbulent water channel flow obstructed with an inserted square rod in the Reynolds number range of $Re \geqq 6{,}000$. An intermittent dye injection method was developed and was effectively used in tracking the motion of the Karman vortex. A hydrogen bubble technique was combined to examine the characteristics of the near-wall flow. Heat transfer experiments were also conducted for the same type of air flow. The main results obtained in this study are as follows.

Since the flow disturbance given by the inserted rod is strong, near-wall flow interacts with the Karman vortex, even when the rod is mounted in the center plane. The near-wall flow structure downstream of the rod is not significantly affected by the detailed difference in the approaching flow to the rod. This explains why the qualitative features of the Nu distribution do not significantly vary with the flow Reynolds number or with the inlet flow condition.

The Karman vortex showed criss-cross motion in the present Reynolds number range. The criss-cross motion of the vortex occurred even when the rod was mounted off the center plane. Asymmetry of the flow does not suppress such criss-cross motion of the vortex. The shedding frequency of the Karman vortex is higher in the present type of confined flow, as compared to the case where the rod is mounted in a uniform flow flowing in large space. The moving speed of the vortex takes a constant value from the position close to the rod and is equal to the cross-sectional averaged velocity.

Three peaks appear in the distribution of the local Nusselt number. The first appears at the insertion position of the rod and is produced by the flow acceleration in the space between the rod and the channel wall. The third appears at the position where the separation shear layer from the upper edge of the rod approaches the channel wall. The generating mechanism of the second peak was discussed in detail, because the appearance of the second peak is the primary cause of the overall heat transfer enhancement. The present flow visualization strongly supports a conjecture that the mechanism suggested previously by Suzuki and Suzuki (1994a) for low Reynolds number range can hold also for the present much higher Reynolds number range. The suggested mechanism is related to the washing action exerted by discrete vorticity islands. Periodical fluctuation of vorticity was actually observed in the near-wall region, and it suggests the appearance of high vorticity region off the channel wall. The high vorticity region is similar in nature to the discrete vorticity island. Flow reversal observed in the space between such a high vorticity region and the channel wall is regarded as a footprint of the washing action. To confirm this conjecture, a quantitative study of the flow structure should be made in near future.

References

Webb, R. L. and Bergles, A. E., 1982. *Performance Evaluation Criteria for Selection of Heat Transfer Surface Geometries Used in Low Reynolds Number Heat Exchangers*, S. Kakac, R. H. Shar and A. E. Bergles. (eds.) Hemisphere, Bristol, PA, 819–842

Hans, J. L. 1983. *Vortex Flow in Nature and Technology*. Wiley-Interscience, New York

Hong Y.-J. and Hsieh S.-S. 1993. Heat transfer and friction factor measurements in ducts with staggered and in-line ribs. *Trans. ASME*, **115**, 58–65

Liou T.-M. and Hwang J.-J. 1992a. Turbulent heat transfer augmentation and friction in periodic fully developed channel flows. *Trans. ASME*, **114**, 56–64

Liou T.-M. and Hwang J.-J. 1992b. Developing heat transfer and friction in a ribbed rectangular duct with flow separation at inlet. *Trans. ASME*, **114**, 565–573

Okajima, A. 1982. Strouhal numbers of rectangular cylinders. *J. Fluid Mech.*, **123**, 379–398

Oyakawa, K. and Mabuchi, I. 1981. Fluid flow and heat transfer in a parallel plate duct containing a cylinder. *Bull. JSME*, **24**, 1795–1802

Oyakawa, K. and Mabuchi, I. 1982. Heat transfer in parallel plate duct with circular cylinders inserted in staggered arrangement. *Bull. JSME*, **26**, 543–553

Senoo, Y. and Yamaguchi, M. 1975. Observation for inner flow of impeller by use of the dye injection. *Turbo Machinery*, **3**, 28, (in Japanese)

Suzuki, H., Inoue, Y., Nishihara, Y. and Suzuki, K. 1991a. Unsteady flow and heat transfer in a channel obstructed by a square rod, (1st Report, validation of numerical calculation and flow visualization of vortex street). *Trans. JSME*, **57**, 1390–1395 (in Japanese)

Suzuki, H., Inoue, Y. and Suzuki, K. 1991b. Unsteady flow and heat transfer in a channel obstructed by a square rod, (2nd report, statistical characteristics and time variation of the Flow), *Trans. JSME*, **57**, 1396–1402, (in Japanese)

Suzuki, H., Suzuki, K., Inoue, Y. and Hagiwara, H. 1991c. Unsteady flow and heat transfer in a channel obstructed by a square rod, (3rd Report, characteristics and mechanism of heat transfer). *Trans. JSME*, **57**, 1403–1409, (in Japanese)

Suzuki, H., Fukutani, K., Takishita, T. and Suzuki, K. 1993a. Unsteady flow in a channel obstructed by a square rod (crisscross motion of vortex). *Int. J. Heat Fluid Flow*, **14**, 2–9

Suzuki, H., Inoue, Y. Nishimura, T., Fukutani, K. and Suzuki, K. 1993b. Heat transfer characteristic in a channel flow obstructed with a square rod mounted in asymmetric positions. *Trans. JSME*, **59**, 1692–1697, (in Japanese)

Suzuki, K. and Suzuki, H. 1994a. Unsteady heat transfer in a channel obstructed by an immersed body. *Annual Review of Heat Transfer*, Vol. 5, C. L. Tien (ed.), CRC, Grand Rapids, MI, 177–206

Suzuki, K. and Suzuki, H. 1994b. Instantaneous structure and statistical feature of unsteady flow in a channel obstructed by a square rod. *Int. J. Heat Fluid Flow*, **15**, 426–437

Yao, M., Nakatani, M. and Suzuki, K. 1988. Flow visualization and heat transfer experiment in a duct with an insertion of a staggered array of cylinders, *Exp. Thermal Fluid Sci.*, **2**, 519–526

Yao, M., Nakatani, M. and Suzuki, K. 1990. Numerical investigation of turbulent heat transfer. *Proc. 67th JSME National Conference*, (in Japanese), 305–306

Yao, M., Nakatani, M. and Suzuki, K. 1994. Flow visualization and heat transfer experiments between two parallel plates with an insertion of a square rod. *Trans. JSME*, **60**, 2819–2825 (in Japanese)